Editors Comment, Referee 1
Report 1

(1) Line 15: use "was performed to search for the possible" instead of "was performed to research the possible"
(2) Thank you for the correction of this grammatical error.
(3) "was performed to search for the possible"

(1) Line 34: use "by spectral analysis" instead of "by spectral analyzing"
(2) Thank you for the correction of this grammatical error.
(3) "by spectral analysis"

(1) Lines 36 and 37: use "small-scale & medium-scale" instead of "small-scaled & medium-scaled"
(2) Thank you for the correction of this grammatical error.
(3) "small-scale & medium-scale"

(1) Line 75: The information introduced on line 75 in order to attend the reviewer comment does not seem very precise. Generally the satellite measurements are not available exactly at the same location as the ground based observations. In those cases the satellite paths that are inside a grid in latitude versus longitude are used instead. Please check what was used in the present case and change the information accordingly.

(1) Lines 99-100 & Figure 1: Reviewer #1 questioned "*What is the feature identified as the gravity wave in the raw or filtered image?*" Although you mention to have improved the resolution of the airglow image in the manuscript, it is still not possible to see the features in the images. Maybe you can upload an image at higher resolution (or a video) as supplementary material which can help the reader to identify the ripples.
(2) A video has been added as a supplement
(3) "For further details on the propagation of ripples, see the video clip in the supplement."

(1) Lines 111-120: The modifications to the text were introduced in order to reply the Reviewer#1 question "Was this done to fill in data gap between 23:51 and 8:35 UT? What about time between 20:00 and 23:46 as most of your gravity waves fall within this period? Also how reliable is your interpolation when you have only a small sample of data to spread over such a long time period?" You mention that you have used the MSIS model for the times and heights for which SABER temperatures were not available. These mean that the statements on lines 119-120 ("outbreak of cold air at heights lesser than 150 km" and "peak period between 17h00 and 19h00 has a temperature value 1000 K") are totally based in MSIS which is an average model. What are the implications of this for the present study?
(2) Thank you for pointing this out. The content has been removed from the article.

(1) Page 7 and Equations 3a-3f: The equations should appear right after the sentence in which they are first mentioned; right after the sentence on lines 148-149 "Considering 3D-space, the wave trajectory can be represented using the dispersion relation as (3a-

3c), also, the refraction of the wave packages can be represented as (3d-3f)"
(2) Thank you for indicating this. The equations have been re-arranged and now appear right
   after the sentence where they were first referred to.

(1) Line 170: use "The spectral results shown in Table 1 show" instead of "The spectral
results shown in Table 1 shows".
(2) Thank you for pointing this out. The corrections have been made.
(3) "The spectral results shown in Table 1 show"

Editors Comment, Referee 2
Report 1
 (1) Lines 42-43: Please rephrase the sentence "Airglow emissions are faint luminescence that
are produced as a result of the emission of solar radiations (ultraviolet and x-
radiation) by ionized air molecules". It could be replaced by "Airglow emissions are faint
luminescence that are produced as a result of the emission of electromagnetic
radiation by excited ionized or neutral atoms or molecules".

(2) Thank you, we have rephrased this in the manuscript.

(1) Line 57: Please use "the current study" instead of "this current study".
(2) Thank you, we have changed this word in the manuscript as well.

(1) Line 67: Please use "The present study" instead of "This present study".
(2) Thank you for your comment, we have reworded these phrases in the manuscript.

(1) Line 74: Use "Ionosphere Mesosphere" instead of "Mesosphere Ionosphere".
(2) This correction has been done, thank you.

(1) Line 106: The parameters listed in Table 1 should be defined (e.g. cH was defined only
on line 244).
(2) We have defined this parameters in the manuscript body, thank you.

(1) Line 107: Please use "the present study" instead of "this present study".
(2) Thank you, we have reworded this phrase and many others in the manuscript.

(1) Lines 141, 143: Please check Equations (1) and (2) as they differ from the ones listed in
Vadas & Fritts (2005).
(2) Thank you, we have corrected this citation, and cited the right author.

(1) Line 150: "equations (3a-3f)" instead of "equations (3a-3d)".

(2) Thank you very much for your correction, the modification has been done.

(1) Line 164: Please check Equation 3e for correctness.
(2) Thank you so much, the error in the denominator has been rectified and the riht equation has been written out in the manuscript.

(1) Regarding equations 3a-3f. These equations are the same described in the work of Marks and Eckermann (1995). In the present work you seem to have followed the methodology described by Vadas and Fritts. Please double check if these are the equations that the code you are using for the ray tracing analysis is solving. If they are not it is better not to include them in the manuscript.
(2) Thank you, we have cited the right publication and article.

(1) Figures 4b to 8b: Please specify the time for which the convective cloud activity was

included in the Figures. This is particularly important for events for which the ray-tracing results show the starting time farther from the gravity wave detected time (e.g.

event #2).
(2) Thank you, this is depicted in the reverse ray tracing figures in the manuscript.

(1) Line 227: ITCZ is first used here. Please write it out "Inter Tropical Convergence Zone (ITCZ)".
(2) Thank you, this we have dont in the manuscript.

(1) Line 271: Please use "gravity wave events" instead of "gravity events".
(2) Thank you, this we have done.

(1) Please check the references. Same authors referenced in the text are not in the Reference List. Some references are incomplete (missing the name of the journal, for example).
You have used more than one format for the references. Please use the Annalles Geophysical format for all of them. The format for references can be found at the website: https ://www. ann ales-geophysicae.net/for_authors/manuscript_preparation.html
(2) The format of the references has been redone, thank you very much.

Investigation of sources of gravity waves observed in the Brazilian Equatorial region on 08 April 2005

Oluwakemi Dare-Idowu[1,2], Igo Paulino[1], Cosme A. O. B. Figueiredo[3], Amauri F. Medeiros[1], Ricardo A. Buriti[1], Ana Roberta Paulino[1,4], and Cristiano M. Wrasse[3]

[1]Unidade Acadêmica de Física, Universidade Federal de Campina Grande, Campina Grande, Brazil.
[2]University of Paul Sabatier, Toulouse, France
[3]Divisão de Aeronomia, Instituto Nacional de Pesquisas Espaciais, São José dos Campos, Brazil
[4]Departamento de Física, Universidade Estadual da Paraíba, Campina Grande, Brazil

Correspondence: Oluwakemi Dare-Idowu (oluwakemidareidowu@gmail.com)

Abstract.

On 08 April 2005, a strong gravity wave activity (of more than 3 hours) was observed in São João do Cariri (7.4° S, 36.5° W). These waves propagated to the southeast and presented different spectral characteristics (wavelength, period and phase speed). Using the hydroxyl (OH) airglow images, the characteristics of the observed gravity waves were calculated; the wavelengths ranged between 90 and 150 km, the periods from ~26 to 67 min and the phase speeds ranged from 32 to 71 m/s. A reverse ray-tracing analysis was performed to search for the possible sources of these detected waves. The ray-tracing database was composed of temperature profiles from NRLMSISE-00 model and SABER measurements and wind profiles from HWM model and meteor radar data. According to the ray path, the likely source of these observed gravity waves was the Inter Tropical Convergence Zone with intense convective processes taking place in the northern part of the observatory. Also, the observed preferential propagation direction of the waves to the southeast could be explained using blocking diagrams, i.e. due to the wind filtering process.

Keywords. Gravity waves, Airglow, Reverse Ray Tracing, Troposphere, Mesosphere, ITCZ.

1. Introduction

Since the publication of the pioneering works of Hines in the 1960s on the detection of irregular motions 'gravity waves' in the upper atmosphere, there have been numerous improvement work-outpours. Gravity waves are results of disturbances that occur in atmospheric fluids with the upper mesosphere and thermosphere region being largely impacted (e.g., Fritts and Alexander, 2003). Potential sources of these waves are cold fonts (e.g Plougonven et al., 2017), troposphere convection (e.g., Vadas et al., 2009), wind shear (e.g Clemesha and Batista, 2008), topography and wave breaking (e.g., Sarkar and Scotti, 2017), as well as solar eclipse (e.g., Marlton et al., 2016). These atmospheric structures have been identified as a key component in the transportation of energy in the mesosphere and lower thermosphere (MLT) region (e.g., Fritts, 1993; Medeiros et al., 2007; Campos et al., 2016).

Internal GWs are generated as adjustment radiations whenever a sudden change in forcing causes the atmosphere to depart from its large-scale balanced state. Such a forcing anomaly occurs during a solar eclipse (Campos et al., 2016; Marlton et al., 2016). The intrinsic properties of the gravity waves (observed horizontal phase speed, propagation direction, observed period, horizontal wavelength) can be calculated directly from the airglow images by spectral analysis. Using the dispersion relation, the vertical wavelength can also be computed (Vargas et al., 2009). Gravity waves can be summarized as large-scale waves, medium-scale waves, and small-scale waves. Small-scale gravity waves are characterized by horizontal wavelengths in tens of kilometers (Medeiros et al., 2003), medium-scale gravity waves propagate at ~ 170 km altitude, and large-scale waves have high phase speeds and travel farther horizontal distances compared to others (Vadas et al., 2009).

40   In the MLT region, there are several and continuous chemical reactions such as the OH airglow emissions (e.g., Sivjee et al., 1992; Taylor et al., 2009; Campos et al., 2016). These emissions among several others have been used by many authors as a proxy for investigating gravity wave activities. Airglow emissions are faint luminescence that are produced as a result of the emission of electromagnetic radiations by excited ionized or neutral atoms or molecules. These luminosity are usually captured by the all sky imagers (ASI) (e.g., Wallace, 1959; Krasovskij et al., 1965).

45   To identify source location of gravity waves, the reverse ray tracing method has been widely adopted. This algorithm allows the identification of the source locations of gravity waves. Several researchers have successfully implemented this technique to identify points of generation of these waves under different atmospheric conditions using airglow images (e.g., Hecht et al., 1994; Brown et al., 2004; Wrasse et al., 2006; Vadas et al., 2009; Pramitha et al., 2014, Sivakandan et al., 2016).

50   Wrasse et al., (2006) did a comprehensive study of gravity waves observed over Brazil and Indonesia and concluded that most of the studied waves have their sources in the troposphere. Similarly, Vadas et al. (2009) studied the propagation of gravity waves observed during the SpreadFEx campaign in Brazil and found out that the likely sources of those waves were deep convection in Brazil. In addition, Pramitha et al., (2014) identified that 64 % of observed GWs over Gadanki, India originated from the upper troposphere while the remaining were seen to have been ducted in the
55 mesosphere. Furthermore, in 2016, Sivakandan et al. (2016) studied Gws observed in the southern part of India and associated the sources to convection.

        The objective of the current study is to extensively study a strong activity of GWs observed in São João do Cariri (7.4^o S, 36.5^0 W) on 08 April 2005. More than three hours of GW activities were observed and the waves propagated exclusively to the southeast. An explanation for this uncommon pattern is presented in this work investigating the
60 combining effect of the location of the source and the wind filtering process.

2. Instrumentation

2.1 The all sky imager

        The GWs detected in this study were observed using the ASI installed at the observatory in São João do Cariri. The ASI is an optical instrument that provides monochromatic maps of aurora and atmospheric airglow emission of
65 different wavelengths. It has been designed to keep track of the spatial and temporal variations of OH, OI5577, 6300 nm airglow emissions (e.g. Paulino et al., 2010).

        The present study however utilized only the OH airglow images captured by the ASI at an altitude of 87 km. This instrument comprises of a fish-eye (f/4) lens, a telecentric lens system, a field of view of 180^0, a computer-controlled filter wheel with several slots for the observation of different emissions, and a charged coupled device (CCD) camera with a
70 CCD device used as a photodetector for increased sensitivity. More technical and operational details about this particular imager at São João do Cariri can be found in Medeiros et al., 2007; Paulino et al. (2012).

2.2 TIMED/SABER Satellite

        The Sounding of the Atmosphere using Broadband Emission Radiometry (SABER) is one of the four instruments onboard the Thermosphere Ionosphere Mesosphere Energetics and Dynamics (TIMED) satellite. The vertical temperature
75 measurements from 20 to 108 km were observed on 08 April 2005 over Sao Joao do Cariri (7.4^o S, 36.5^o W) from this instrument, SABER. In the study, the vertical temperature measurements from 20 to 108 km were obtained from SABER. Data from the Naval Research Laboratory Mass-Spectrometer-Incoherent-Scatter (NRLMSISE00) atmospheric model (Picone et al., 2002) was utilized for complementing the measurements at unavailable heights of 0-19 km, and 109-400 km.

These measurements were used to provide vertical profiles of kinetic temperature, pressure, geopotential height, and

80 volume mixing ratios for the trace species (Mertens et al., 2001).

2.3 The SKiYMET Meteor Radar

The All-Sky Interferometric Meteor Radar (SKiYMET) system located at 7.4° S, 36.5° W provided measurements of the horizontal wind speeds and direction of the mesosphere (81-99 km). The radar which is composed of Yagi antennas-5 receiving antennas and one transmitting antenna operates at 35.24 MHz with a maximum power of 12 kW. This instrument detects the trail left behind by vaporized meteors, determines the angle-of-arrival by using the phase difference between the receiving antennas, then measures the radial velocity by using the derivation of the speed and direction of the atmospheric winds carrying the meteor trail at a specified altitude. The phase delay between the transmitted and received signal is used to determine the position of the trail. Further detail about this radar has been published in (e.g., Hocking et al., 2001; Egito et al., 2018; Paulino et al., 2015).

3. Methodology and data analysis

3.1 Determination of gravity waves parameters

To obtain the characteristics of the detected gravity waves, a two- dimensional Fast Fourier Transform (FFT) was used in specified batches of OH airglow images. The pre-processing of the airglow images can be summarized in the following procedures:

- Rotating the image to fit the top of the image with the north geographic region;
- Removing low frequency waves by applying the Butterworth high pass filter;
- Contrast enhancement and unwarping the airglow images for FFT analysis.

Figure 1(a) shows one of the raw OH image obtained from the ASI in Observatorio de Luminescencia Atmosferica de Paraiba (OLAP). This image is a typical example of the wave events observed on this night. The ripples enclosed in the red box in Figure (1a) represents the gravity wave structure. This particular event was captured by the ASI at ~23:58 UT on 08 April 2005. This image however was contaminated with stars (bright circles), and the Milky Way (white streak running from the bottom North-West to South-East direction), tree branches/leaves (East-edge of the image), and building tops shown by the red arrow. Figure 1(b) portrays a clearer image after image processing. Figure 1(c) represents the unwarped version of previous image. The last figure shows the spectrum of the encapsulated event. The bright red circle which depicts the amplitude of the gravity wave and its positioning also provides the propagating direction of the wave. Table 1 presents a summary of all the wave events observed on this night. Additional information about the cross spectrum analysis used in the present study to obtain the characteristics of these waves can be found in (Wrasse et al., 2006).
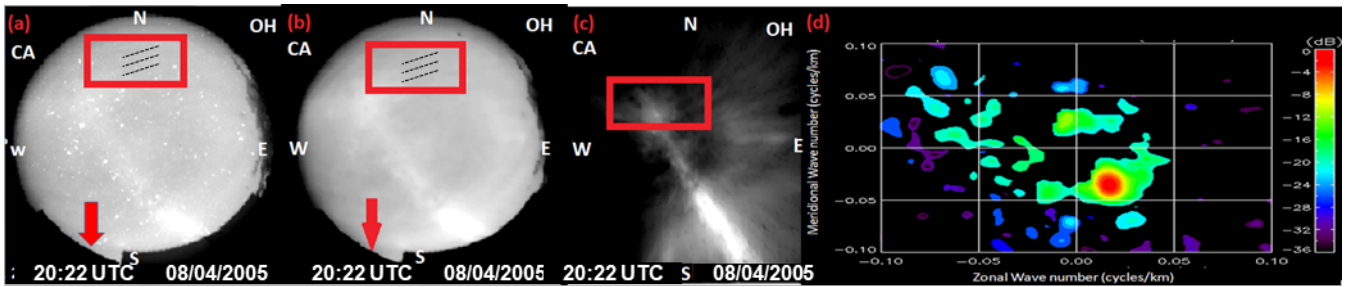
Figure 1: Illustration of the image processing. (a) Raw OH image collected from the ASI in São João do Cariri on 08 April 2005. For further details on the propagation of ripples, see the video clip in the supplement. (b) Filtered image (c) Unwarped and rotated image of the gravity wave event inside the red box area in previous images for FFT analysis (d) Cross spectrum applied to the GW enclosed in the box in (c).

Table 1*: The observed properties of the 5 wave events

Event	Time (UTC)	τ (min)	λ_H (km)	Propagation direction (^{o})	cH (ms−1)
01	20:22	26.3	90.2	139.8	57.2
02	21:33	66.9	144.5	131.2	36.0
03	22:56	64.2	125.8	125.0	32.7
04	23:29	40.8	142.0	142.0	58.0
05	23:58	35.0	149.2	150.9	71.0

3.2 The atmospheric profile

The SABER instrument provided temperature measurement from 23h46 to 23h51 UT on 08 April, and from 08h35 to 08h40 UT on 09 April for altitudes 20-108 km. Then, linear interpolation between 23h46 (08 April) and 08h40 (09 April) was done for the same altitude range. In addition, numerical values for temperature were obtained from https://omniweb.gsfc.nasa.gov/vitmo/msis_vitmo.html for time (12h to 22h) on 08 April 2005 and for missing heights of (0-19km, 109-400km) to complement the SABER measurements. Finally, a 13-profile temperature data with a temporal resolution of 2hrs was constructed for the whole period. However, some discrepancies were at the combining points, hence the data were smoothened so that the model can seamlessly match the measurements at these junctions. This methodology was discussed by Paulino et al. (2012).

The SKYiMET radar provided the zonal and meridional wind measurements from 81-99 km every 3 km from 0h to 23h on 08 and 09 April 2005 with a resolution of 1h. Similarly, numerical interpolation provided the spatial resolution of the wind with a 2 hours resolution like the temperature- with supporting data from the Horizontal Wind Model (HWM) (Drob et al., 2008) from 0 km to 80 km, and above 100 km.

From the temperature and wind measurements, other atmospheric parameters representing the atmospheric state of the period of study were obtained. The pressure $P(z) = P_o \exp\left(-\int_0^z \frac{g}{RT} dz'\right)$ was obtained using a combination of the ideal gas law $P = R\rho T$ and the hydrostatic balance equation $\frac{dP}{dz} = -g\rho$ where ρ is the density obtained from https://omniweb.gsfc.nasa.gov/vitmo/msis_vitmo.html, and the molecular weight was estimated from

$$X_{MW} = \frac{1}{2}\left(X_{MW0} - X_{MW1}\right)\left[1 - \tanh\frac{s-a}{\Delta_a}\right] + X_{MW1}$$ where X_{MW0}, X_{MW1}, Δ_a and a are constants given by 28.90, 16.0, 4.20, and 14.90 respectively, while $s = \ln\rho$ (Vadas et al., 2009). Additional details about the reverse-ray tracing parameters can be found in (Vadas et al., 2007; Vadas et al., 2009), T is the temperature, **g** is the acceleration due to gravity, $R = \frac{8314.5}{X_{MW}}$ is the gas constant, z is the altitude, and P_o is the static pressure.

The scale height $H = -\rho / d\rho / dz$ is obtained from the ratio of the density to the derivative with respect to the altitude, while the potential temperature is $\theta = T\left(P_o / P\right)^{R/C_P}$, C_p is the specific heat capacity at constant pressure, and the Brunt–Väisälä frequency is $N = \sqrt{\left(\frac{g}{\Theta}\frac{d\Theta}{dz}\right)}$. See further details in Vadas et al., (2007).

3.3 The Reverse Ray Tracing technique

Every gravity waves gets influenced by the atmospheric winds with velocity **V** = (U, V, W) according to the following equations: Equation 1 describes the ray path while the refraction of the wave vector along the ray path is explained by equation 2. The tracing model employed in the study is based on Lighthill, 1978.

$$140 \quad \frac{dx_i}{dt} = -k_j \frac{\partial V_j}{\partial x_i} - \frac{\partial \omega_{Ir}}{\partial x_i} \tag{1}$$

and

$$\frac{(dk_i)}{dt} = -V_i + \frac{(\partial \omega_{ir})}{k_i} = -V_i + c_{gi} \tag{2}$$

U, V, W, are the zonal, meridional, and vertical wind components respectively, x_i is the spatial position of the wave according to the spatial component $'i'$, ω_{Ir} is the real part of the intrinsic frequency obtained using the dispersion relation in 145 Equation 3 of (Pramitha et al., 2014), and c_g is the group velocity.

Considering 3D-space, the wave trajectory can be represented using the dispersion relation as (3a-3c), also, the refraction of the wave packages can be represented as (3d-3f).

$$\frac{dx}{dt} = U + \frac{k\left(N^2 - \omega_{Ir}^2\right)}{\omega_{Ir}\Delta} \tag{3a}$$

$$\frac{dy}{dt} = V + \frac{l\left(N^2 - \omega_{Ir}^2\right)}{\omega_{Ir}\Delta} \tag{3b}$$

$$150 \quad \frac{dz}{dt} = \frac{-m\left(\omega_{Ir}^2 - f^2\right)}{\omega_{Ir}\Delta} \tag{3c}$$

$$\frac{dk}{dt} = -k\frac{\partial U}{\partial x} - l\frac{\partial V}{\partial x} - \frac{1}{2\omega_{Ir}\Delta}\left[\frac{\partial N^2}{\partial x}\left(k^2 + l^2\right) - \frac{\partial \alpha^2}{\partial x}\left(\omega_{Ir}^2 - f^2\right)\right] \tag{3d}$$

$$\frac{dl}{dt} = -k\frac{\partial U}{\partial y} - l\frac{\partial V}{\partial y} - \frac{1}{2\omega_{Ir}\Delta}\left[\frac{\partial N^2}{\partial y}\left(k^2 + l^2\right) - \frac{\partial \alpha^2}{\partial y}\left(\omega_{Ir}^2 - f^2\right)\right] - \frac{f}{\omega_{Ir}\Delta}\frac{df}{dy}\left(m^2 + \alpha^2\right) \tag{3e}$$

$$\frac{dm}{dt} = -k\frac{\partial U}{\partial z} - l\frac{\partial V}{\partial z} - \frac{1}{2\omega_{Ir}\Delta}\left[\frac{\partial N^2}{\partial z}\left(k^2 + l^2\right) - \frac{\partial \alpha^2}{\partial z}\left(\omega_{Ir}^2 - f^2\right)\right] \tag{3f}$$

where $\Delta = k^2 + l^2 m^2 + \alpha^2$ and $\alpha = \frac{1}{2}H$. k, l, m represents the zonal, meridional, vertical wave numbers respectively, and H 155 is the density scale height (Pramitha et al., 2014). Numerical integration of the six ordinary differential equations (3a-3f) was performed using Runge-Kutta fourth order (Press, 2007). All the observed and intrinsic properties of the gravity waves and parameters representing the atmospheric condition were fed into the reverse ray-tracing (RRT) model. The four stopping conditions imposed constantly checks the horizontal phase speed with the background winds. When any of the condition is violated, the ray tracing integration is terminated. The main stopping criteria are: (i) if the group velocity of 160 the gravity wave is close to the speed of sound ($c_g >= 0.9c_s$); (ii) when the real part of the intrinsic frequency tends to zero ($w_{Ir} \to 0$); (iii) when the vertical wavelength greater than viscosity length or dissipation of the gravity waves. (iv) If the momentum flow of the gravity wave $u_{GW}w_{GW}(z,t) \geq 10^{-5}u_{GW}w_{GW}$ at the height of OH airglow (87km). Extensive

detail of the reverse ray tracing algorithm employed in this study has been published by Paulino et al., 2012; and Pramitha et al., 2014.

## 4. Results and discussions

4.1 Spectral Analysis Result

The spectral results in Table 1 shows observed wavelengths have a standard deviation of 24 km (not shown) and mean value of 130 km with a large amount of variability among the detected waves. This result agrees with the reports of Medeiros et al., (2007) for waves detected at this observatory. Thus, it can be confidently concluded that the observed wavelengths are good representatives of the gravity waves in this observatory.

Figure 2 shows the traveling direction of the 5 events. From the polar chart, it is seen that all the waves are propagating Southeast with an approximate azimuth of ~134° from the north. This is in favorable agreement with the results obtained from previous studies for the same observatory (Essien et al. 2018). This anisotropicity will be discussed later on in this study.
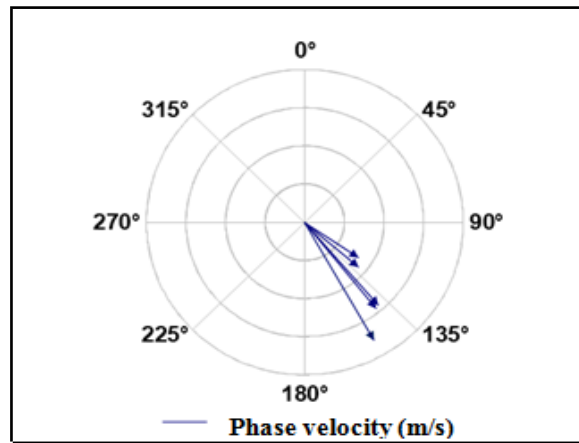
Figure 2: Compass graph showing wave velocities and direction of propagation- each circle denotes a velocity of 20m/s.

Figure 3 shows the impact of the atmospheric wind on the period of the waves. It reveals the difference between the intrinsic period of the waves which lacks atmospheric impact and the observed period which is susceptible to the influence of the atmospheric-winds. However, it can be seen that the winds accelerated almost all the gravity waves. The fluctuation in the period can be attributed to the variability of the horizontal winds. When the gravity wave is traveling anti-parallel to the wind direction, the second term on the left side of this equation $\omega_I = \omega_o - k_H . V_{GW}$ would become negative, consequently forcing the observed frequency to be smaller than the intrinsic frequency, this invariably results in increased observed periods.

8
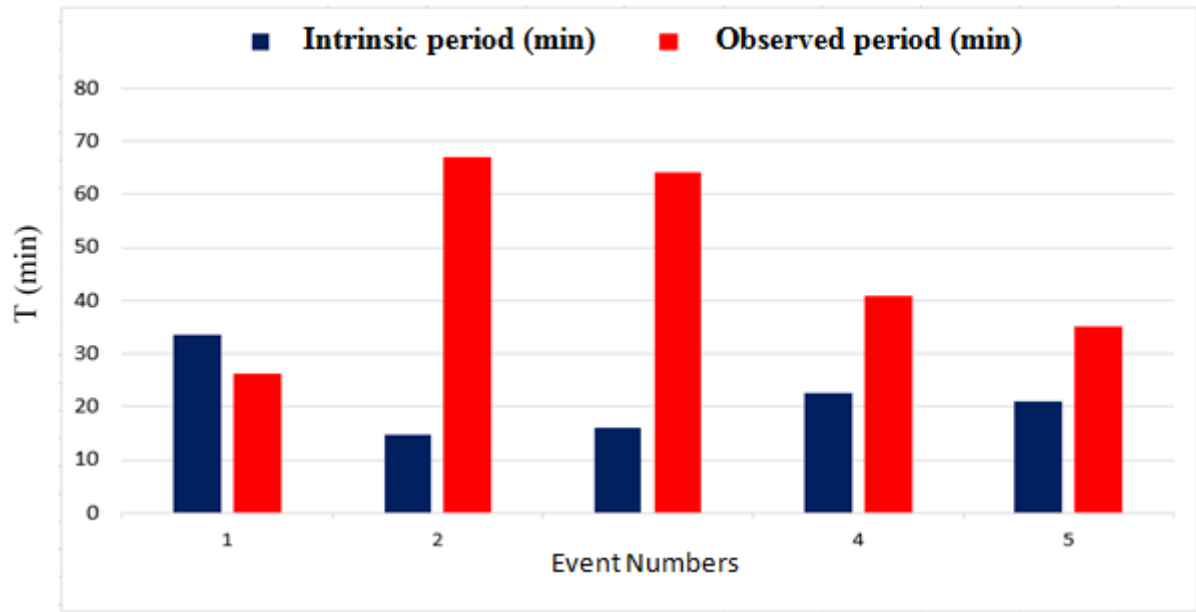
Figure 3: Bar chart graphs of intrinsic and observed periods.

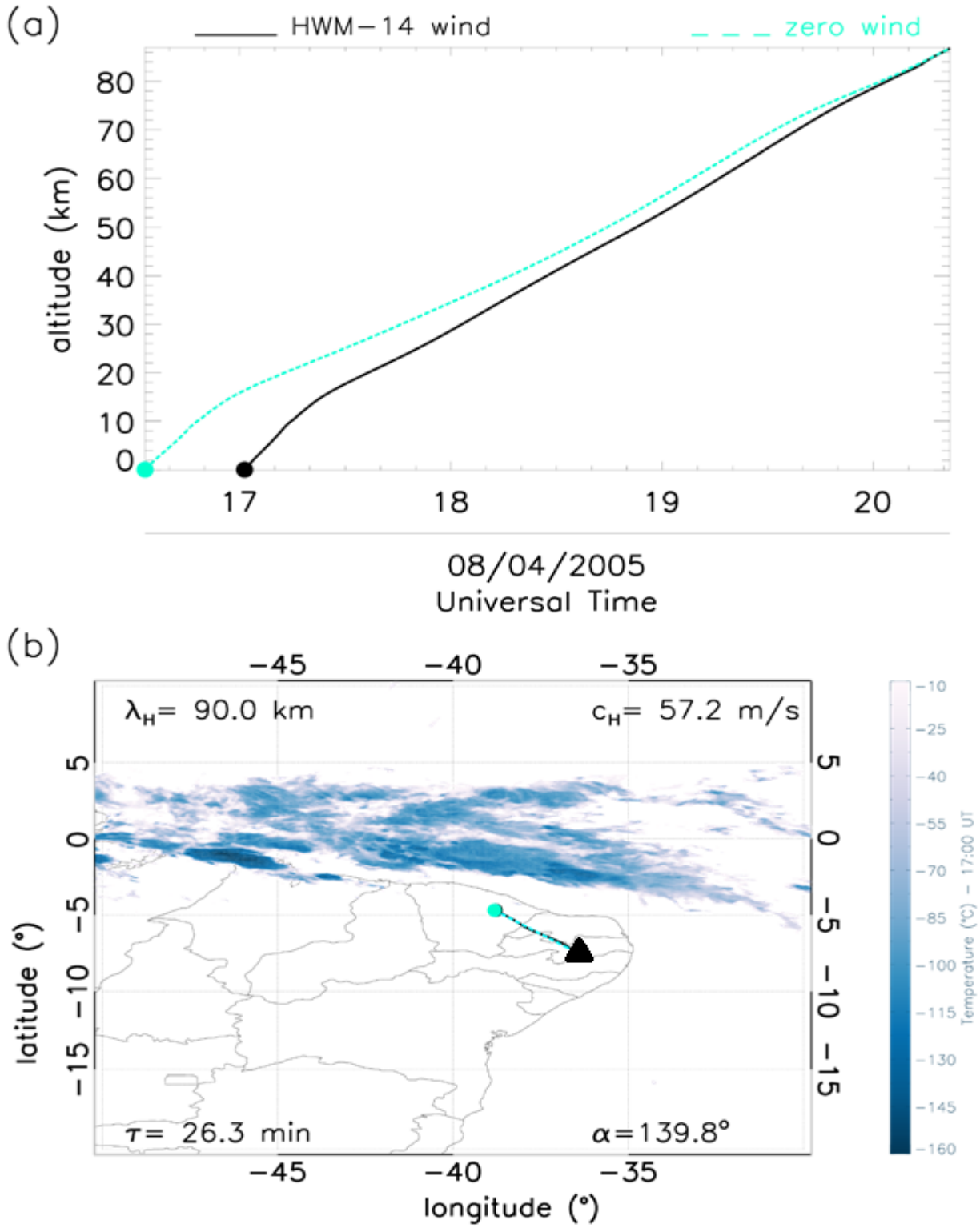### 4.2 Reverse ray-tracing

185   These 5 waves have different spectral characteristics and they were all observed at different times as well. Using the reverse ray tracing technique to back trace these gravity waves from the point of observation in the airglow layer to their source of generation, we present the following results of the RRT analysis. During the backward tracing, we assumed critical levels are not encountered as explained in section 3.3.

        The a-panels of Fig. (4-8) are the ray-paths as a function of the altitude and time and it describes the influence of
190 various wind conditions on each GW event. The light blue line indicates the trajectory of the gravity wave under zero wind influence, while the black line shows the travel path of the wave under the HWM wind influence. This gave a better understanding of the roles played by the atmospheric winds in the traveling paths of GWs from the middle to the lower atmosphere. The blue and black shaded circles represents the time of generation of these waves under zero and modeled wind scenarios respectively. The dashed blue and solid black lines represents the trajectory of the waves under the zero
195 winds and modeled winds conditions respectively.

        The b-panels of Figure 4-8, however, describe the wave path as a function of longitude-latitude; thus providing a closer view of the exact generation point of these waves linearized over the map. The dark blue clouds represent the corresponding convective processes observed at the exact time that these gravity waves were detected. The black shaded triangle represents the precise location of the ASI at the OLAP.

200   Figure 4(b) shows a gravity wave propagating southeastward. Under the modeled wind conditions, this wave was generated at 17h00 UT of the same day, while under zero wind influence, it was triggered at 16h30 UT. Thus, the atmospheric winds were favorable as it accelerated the travel speed. The b-panel of Figure 4 zooms in on the actual source point of this wave. With a horizontal wavelength of 90 km, and phase velocity of 57.2 m/s, the reverse ray tracing result points to the source being in the northern region of the detection point (OLAP). Even though, the HWM-14 winds and zero
205 winds are not equal, the gravity waves propagated through a similar path under both wind condition. Below 70 km, the GW propagates rapidly in the southeast direction which could be due to the strong winds.

9

Figure 4: Reverse ray trace results for GW 1 (a-panels: Altitude as a function of time. Dashed blue and solid black lines show the ray paths for the zero winds and modeled winds respectively, and the time cross section with zero wind and modeled winds. (b-panels: Latitude-longitude cross section over convective cloud activities). Black and blue dots show the location of sources for zero winds and modeled winds respectively. The black triangle represents the exact location of the ASI, while the blue plumes represent convective activities in the region.

Similarly, the ray-tracing results show backward propagation of the second wave event detected at 21h33 UT in Figure 5(a). This shows a similar analysis when compared to the first wave event. However, this wave suffered greater wind 210acceleration ~12 hours as did GW_3 ~10 hours. Thus, just as in GW_1, both GW_4 and GW_5 were accelerated by the modeled winds just by ~ 2 hours and 1 hour respectively.

10
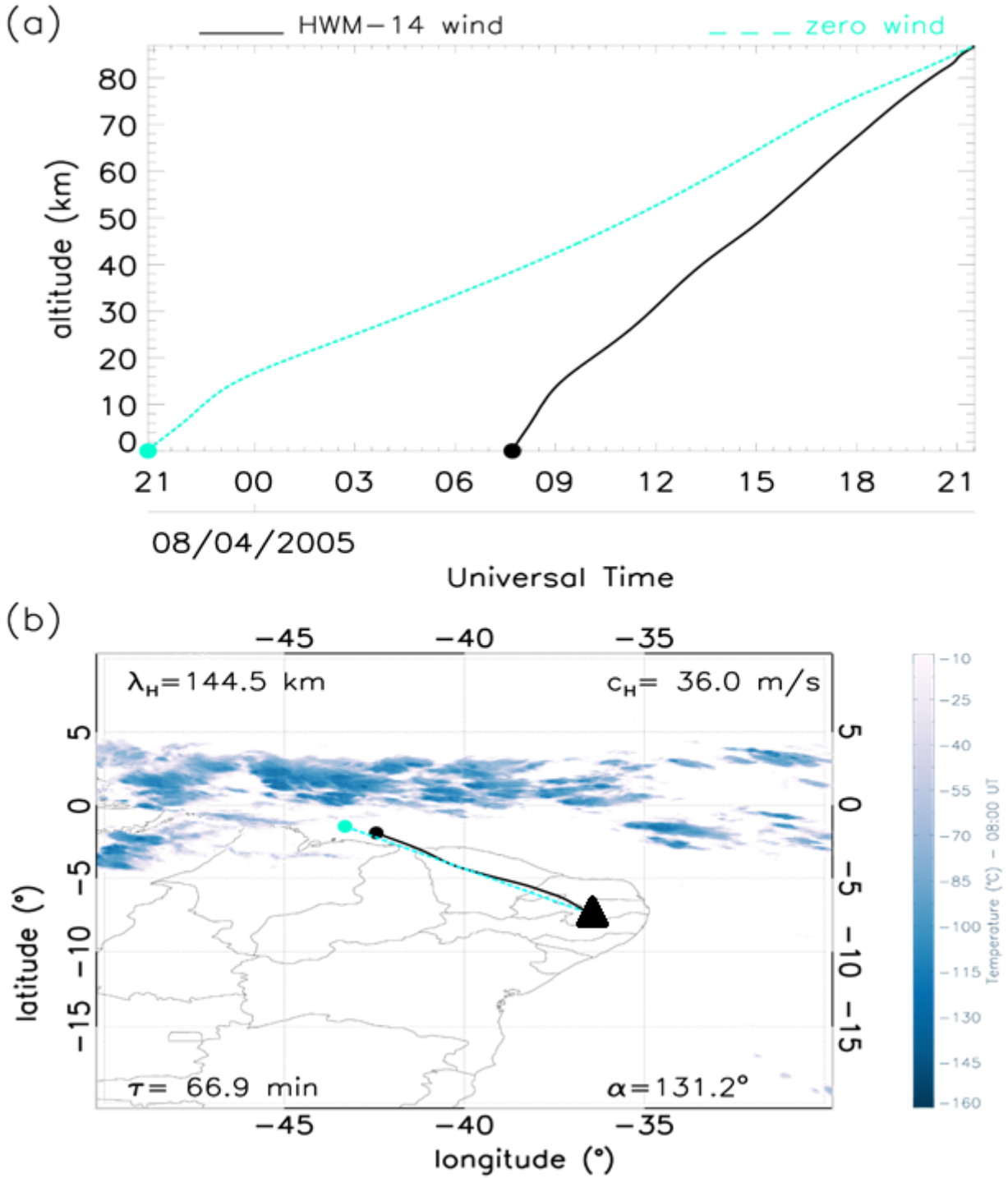
Figure 5: Same as in Figure 4 but for Event #2.

It was observed that the events 2, 3, 4, and 5 with a mean horizontal wavelengths of 140 km propagated more than ~1300 km from their source region. All these 4 events are believed to have originated from the same source due to the resemblance in their characteristics. In Event 1, in comparison to others, the bottom side of the convective sources (deep blue clouds) appear to be farther from the point where we traced the gravity wave source (black and blue dots). However, this particular wave is still linked to the convective processes as its source. According to Vadas and Fritts, 2009 the actual convective area is usually larger than the cloudy areas
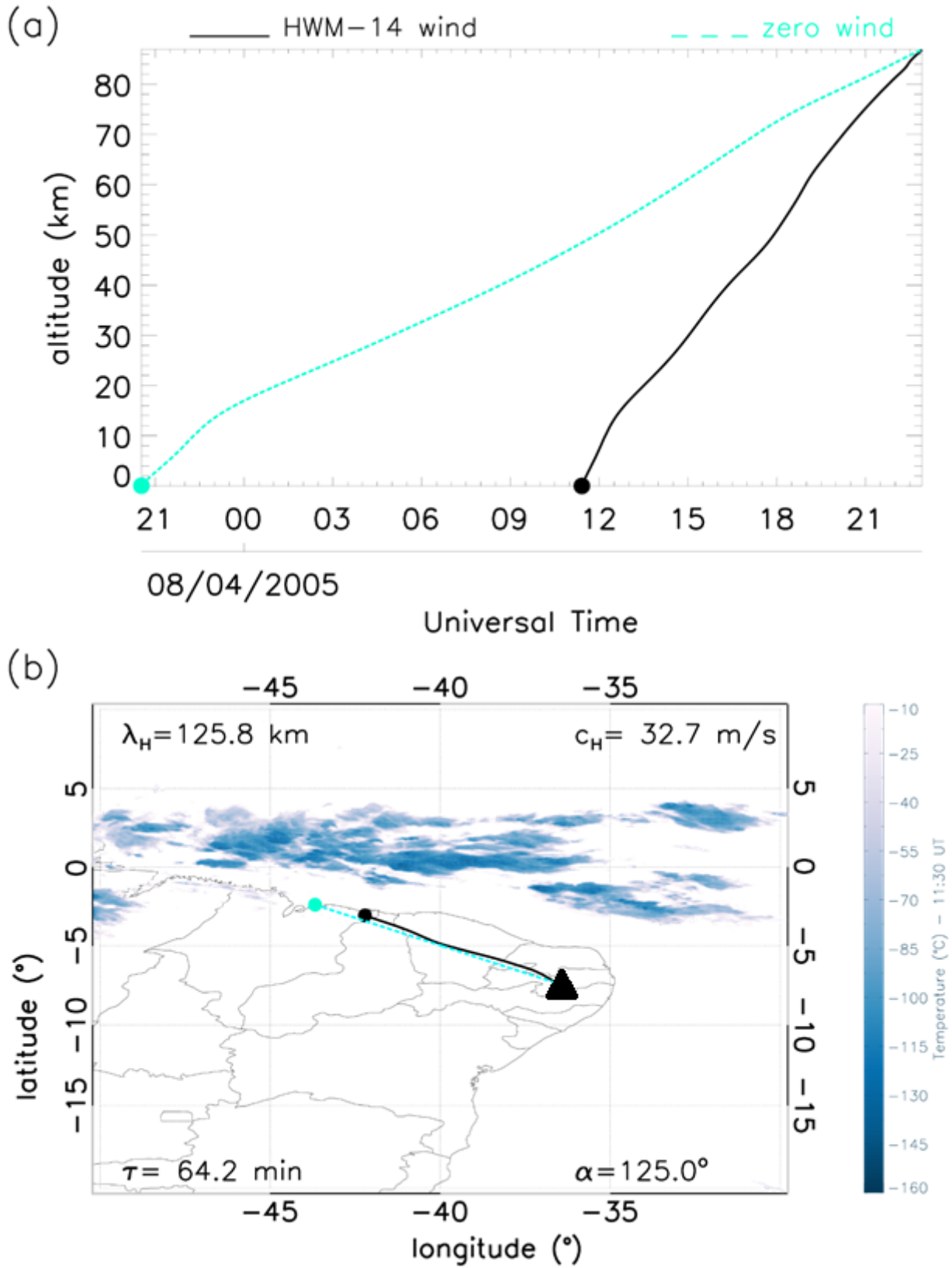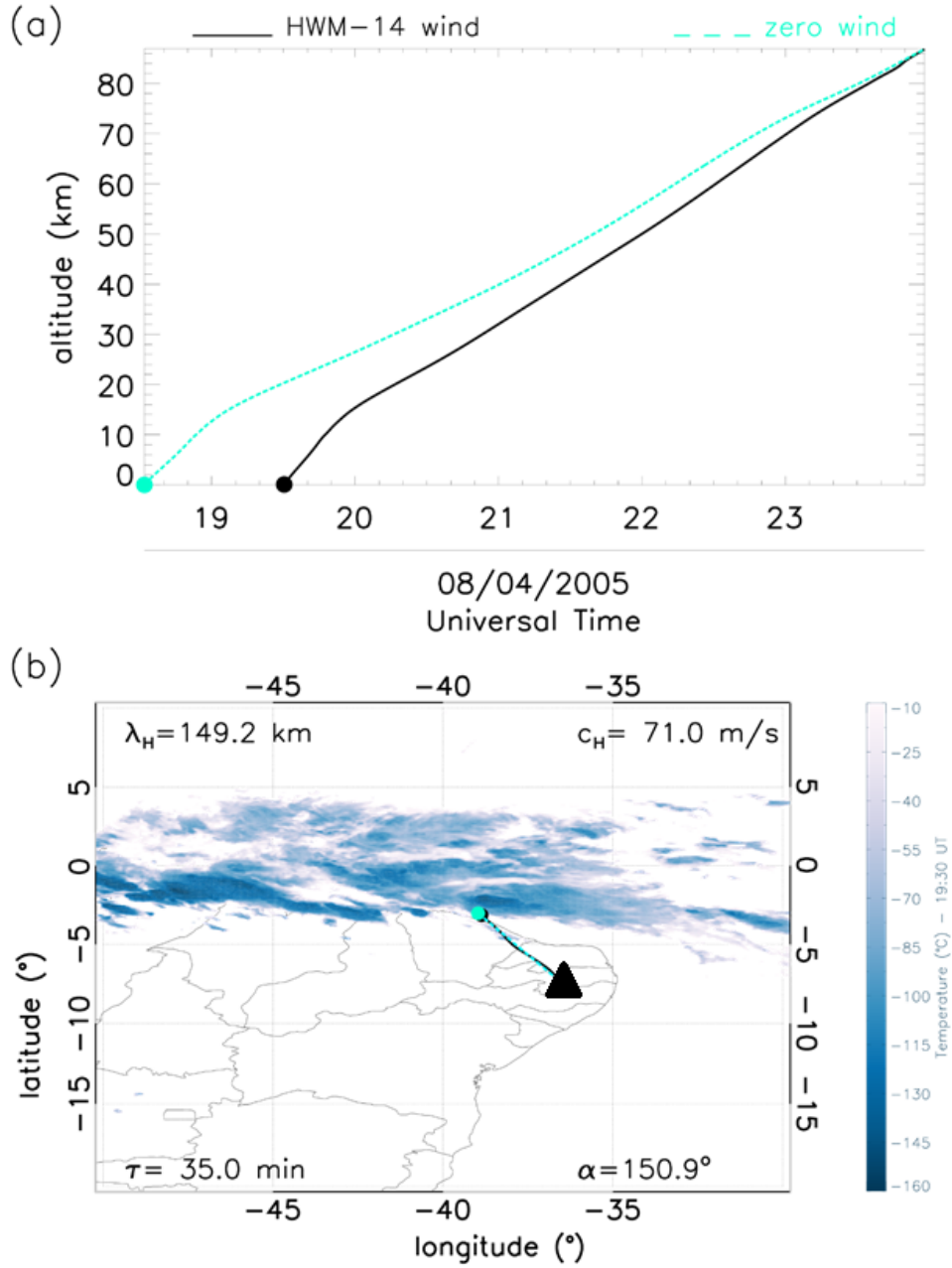
Figure 6: Same as Figure 4, but for the Event #3

Figures 4(b)-8(b) showed the ray paths for the wave events considering the normal and zero wind conditions. In the first panel of event 3, zero wind condition was applied, (blue line) and the modeled wind condition (black line) with a horizontal wavelength of 90 km, phase velocity of 57.2 m/s, propagating angle of 139.8°, 26.3-min period and a vertical wavelength of 90.2 km. It can be noticed in panel (a) of Event #3 that the GW attained the 87 km height for both wind conditions. A slight shift can be observed as there is similarity between both conditions.
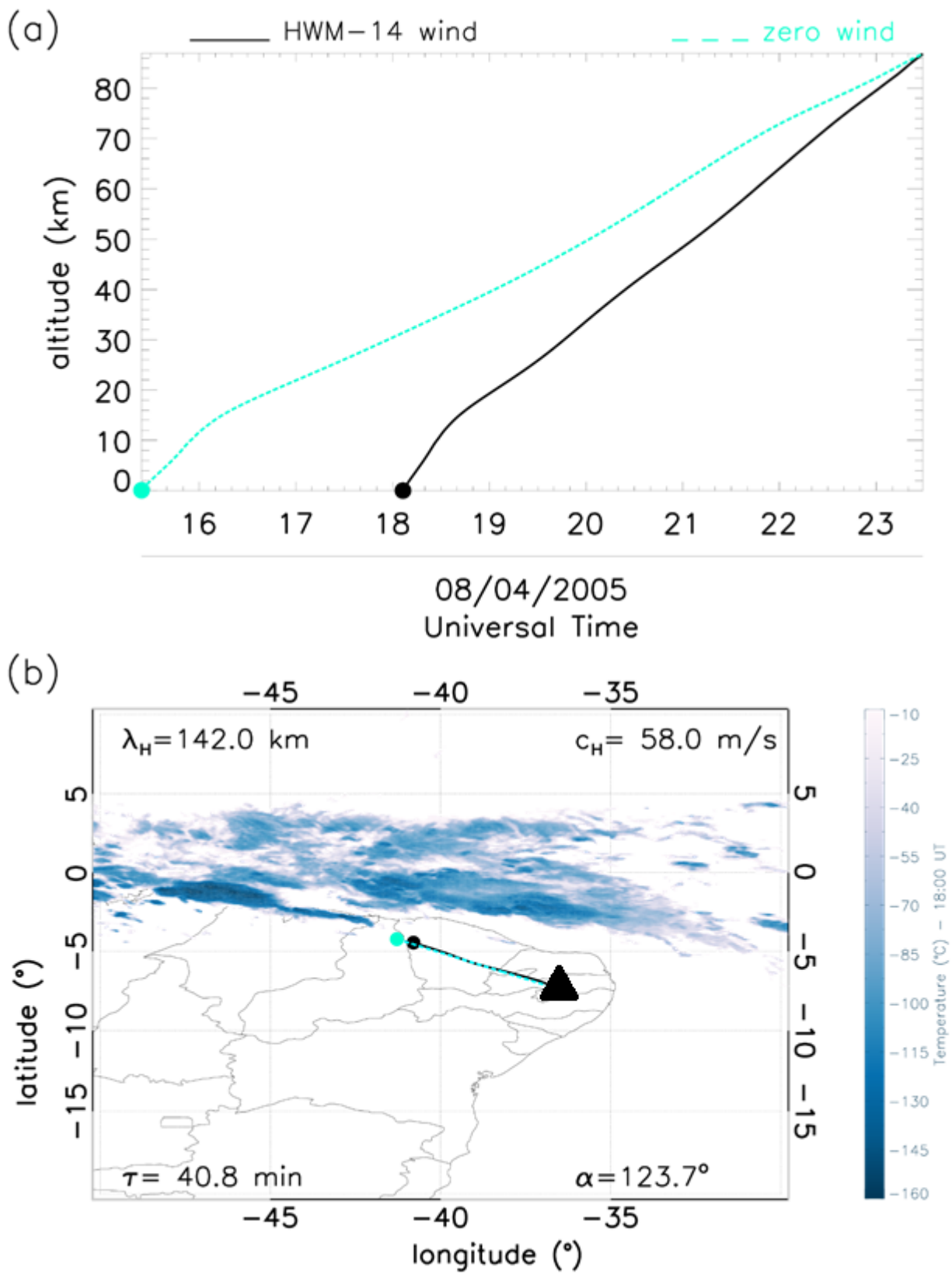
Figure 7: Same as Figure 4 but for Event #4.

**Figure 8**: Same as Figure 5 but for event #5.

All the 5 wave events were reverse traced to some convection activities occurring in the northern region of the OLAP observatory. These have been identified as possible generators of these waves. One question is evident, why is the propagation direction of all the waves southeastward, since the Inter Tropical Convergence Zone (ITCZ) extends horizontally and covers the northern-region of the observatory? These results are in close agreement with previous results of different studies obtained at this laboratory (e.g., Medeiros et al., 2003 and Essien et al., 2018). It is expected that the gravity waves should propagate across all directions in accordance to the location of the ITCZ. Thus, further investigation was done to explain this anisotropy phenomenon. To better understand the physical mechanism that is producing the anisotropy, blocking diagrams have been used to investigate the role of the wind in the filtering process of these gravity waves.

Atmospheric winds are the default features of a real atmosphere. As these gravity waves propagate in the wind direction into the upper atmosphere, they would be susceptible to the Doppler's effect and critical level dissipation (Bretherton, 1966). The critical level marks the region where the horizontal wind component annuls the wave's horizontal phase speed (Medeiros et al., 2003). This region is very important as it decides how and if a traveling wave would

14

235 propagate further. To understand the anisotropy of these GWs, we apply the critical level theory of the atmospheric gravity waves filtering (Fritts and Geller, 1976; Fritts, 1979). From Gossard and Hooke (1975) relation, the intrinsic frequency of the gravity wave under the influence of both horizontal wind components can be described by equation 4 below.

$$\omega_I = k.(c-V) \tag{4}$$

where k is the magnitude of the horizontal wave vector, **V** represents the two horizontal wind components, and c is the 240 horizontal phase speeds of the gravity waves. Equation (4) can also be re-expressed in terms of the zonal and meridional components. Further details can be found in the works of Medeiros et al. (2003), Campos et al. (2016) and Paulino et al. (2018). According to $cH = U cos\varnothing + V sin\varnothing$, where cH represents the phase speeds of these waves, U is the zonal wind component and V is the meridional wind component, we constructed blocking diagrams using the azimuthal angles (ø). With input winds from the Horizontal Wind Model, we aimed to understand the wind filtering effects on the gravity 245 waves, investigate why all the waves have a preferential propagation direction, and also to detect regions where the phase speed of the GW is ≤ the velocity of the winds. The results of the 3-D blocking diagrams are shown in the following figures.

15
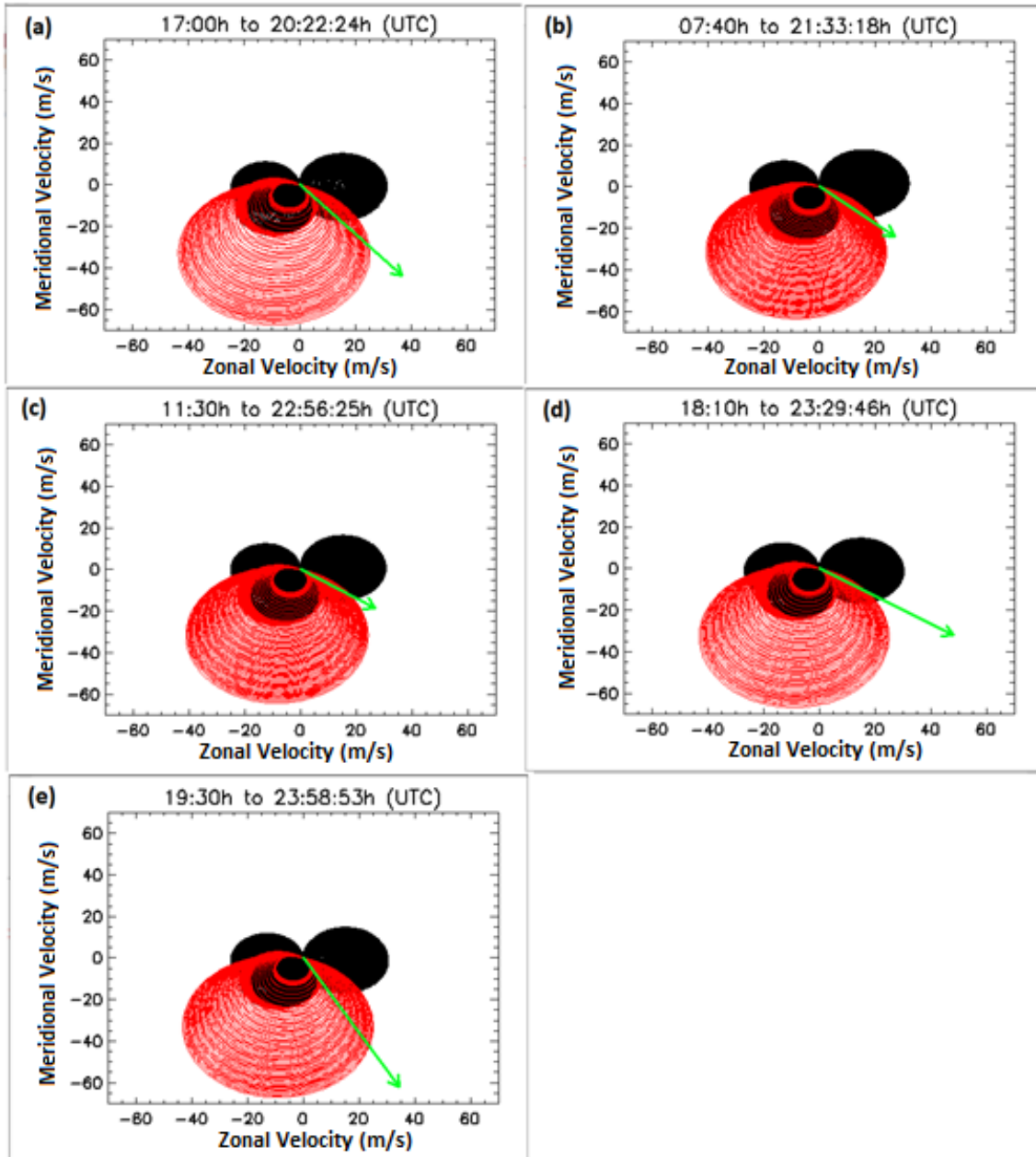
Figure 9: (a) Two-dimensional blocking diagrams for GW #1, (b) GW #2, (c) GW #3, (d) GW #4, and (e) GW #5 events observed at the OH layer (87 km). The green arrow depicts the magnitude and direction of the phase velocity of each gravity wave. The meshed region in red and black represents the magnitude and the direction of the restricted area for the propagation of the wave to the (OH) layer.

Constructing a polar chart as a function of the azimuthal angles and phase speeds using the wind data from HWM and the SkiYMET radar, we show where the phase speeds of these gravity waves equaled the wind speed of the background. The critical levels were projected into the blocking diagram showing for each horizontal wind speed and azimuths of the corresponding GWs. If the phase speed of the GW is trapped in the blocking lines, it represents that the wave is prohibited to propagate upwards.

The above blocking diagram allows the detection of regions where $\omega_I \leq 0$ on the night of 08 April 2005 for the OH emission layer. Every circle in this diagram shows the critical level of the vertical propagation of these waves. The red and black mesh signify the measured and modeled wind components respectively while the green arrow represents the magnitude and direction of the detected GW. The theory of filtering process of gravity waves disallows waves propagating into the shaded region due to the effect of the critical levels (Paulino et al. 2018).

Similarly, we observed that the phase velocity of all the GW events were indeed greater in magnitude than the blocking area. They had strong speed and momentum, enough to escape and propagate through the critical levels easily. It is important to note the main contributions to the blocking area were due to the measured wind in the mesosphere and lower thermosphere, making this analysis strongly confident.

Thus, these detected waves avoided and escaped absorption in the forbidden regions by traveling at these interesting angles. The anisotropy of these waves furthermore compels the source location of the wave to be in the Northwest because the location of this wave source played a key role in this preferential traveling (Fritts et al., 2008; Campos et al.; 2016). The sources of these waves were identified as the convective processes in the ITCZ zone.

5. Conclusions

Using OH airglow images captured by the ASI at São João do Cariri, we investigated the sources of some gravity waves observed on the night of 08 April 2005 in the OH airglow layer. Using the spectral analyzing method, we obtained the characteristics of 5 major gravity wave events with horizontal wavelengths concentrated between 90 km and 149 km. The phase speeds were distributed between the range of 32 m/s and 71 m/s, and the observed periods extended from 26 min to 67 min. These waves presented spectral characteristics that are very compatible with waves previously observed in the same site. In addition, southeast propagation suggested possible sources in the northwest of the observatory.

Focusing on the possible sources of these waves, we back-traced the trajectory of each of these waves from the OH layer $\left(87\,km\right)$ into the troposphere using the meteor radar wind data, the HWM model winds, and zero winds. We found out that the RRT put the source as active convective processes (in the ITCZ) in the northwest of the laboratory as shown in the back tracing results presented above. However, the ITCZ was extended by a long strip in the northern part of the observatory which suggested generation of other GWs that should have been observed in the south and southwest of the observatory. Thus, the construction of blocking diagrams showed that only the spectrum of waves with propagation to the southeast were able to propagate vertically to altitudes of the OH layer. Therefore, the filtering effect of gravity waves was decisive for explaining the presence of observed waves propagating to the Southeast.

285 radar, and revised the manuscript. RAB and AFM have revised the full text. CMW has provided the spectral analysis for the observed gravity waves.

References

Bretherton, F. P.: The propagation of groups of internal gravity waves in a shear flow, Journal of the Royal Meteorological Society, 92(394), 466–480, https://doi.org/10.1002/qj.49709239403, 1966.

295 Brown, L. B., Gerrard, A. J., Meriwether, J. W., and Makela, J. J.: All-sky imaging observations of mesospheric fronts in OI 557.7 nm and broadband OH airglow emissions: Analysis of frontal structure, atmospheric background conditions, and potential sourcing mechanisms, Journal of Geophysical Research, 109(19), https://doi.org/10.1029/2003JD004223, 2004.

Campos J. A. V., Paulino, I., Wrasse, C. M., Medeiros, A. F., Paulino, A. R., and Buriti, R. A.: Observations of small-scale gravity waves in the equatorial upper mesosphere, Revista Brasileira de Geofisica, 34(4), 300 https://doi.org/10.22564/rbgf.v34i4.876, 2016.

Clemesha, B., and Batista, P.: Gravity waves and wind-shear in the MLT at 23°S, Advances in Space Research, 41, 1472 – 1477, https://doi.org/https://doi.org/10.1016/j.asr.2007.03.085, 2008.

Drob, D. P., Emmert, J. T., Crowley, G., Picone, J. M., Shepherd, G. G., Skinner, W., Hays, P., Niciejewski, R. J., Larsen, M., She, C. Y., Meriwether, J. W., Hernandez, G., Jarvis, M. J., Sipler, D. P., Tepley, C. A., O'Brien, M. S., Bowman, J. R., 305 Wu, Q., Murayama, Y., Kawamura, S., Reid, I. M., and Vincent, R. A.: An empirical model of the Earth's horizontal wind fields: HWM07, Journal of Geophysical Research (Space Physics), 113, 12 304, https://doi.org/10.1029/2008JA013668, 2008.

Egito, F., Buriti, R. A., Medeiros, A. F., and Takahashi, H.: Ultrafast Kelvin waves in the MLT airglow and wind, and their interaction with the atmospheric tides, Annales Geophysicae, 36, 231-241. https://doi.org/10.5194/angeo-36-231-2018, 2018

310 Essien P., Paulino, I., Wrasse, C. M., Campos, J. A. V., Paulino, A. R., Medeiros, A. F., and Buriti, R. A.: Seasonal characteristics of small- and medium-scale gravity waves in the mesosphere and lower thermosphere region over Brazilian equatorial sector, Annales Geophysicae, (Submetid), 1–26, https://doi.org/10.5194/angeo-36-899-2018, 2018.

Fritts, D. C.: The excitation of radiating waves and Kelvin-Helmholtz instabilities by the gravity wave-critical level interaction, J. Atmos. Sci., 36, 12–23, https://doi.org/10.1175/1520-0469(1979)036<0012:TEORWA>2.0.CO;2, 1979.

315 Fritts, D. C., and Alexander, M. J.: Gravity wave dynamics and effects in the middle atmosphere, Reviews of Geophysics, 41, https://doi.org/10.1029/2001RG000106, 2003.

Fritts, D. C., and Geller, M. A.: Viscous stabilization of gravity wave critical level flows, J. Atmos. Sci., 33, 2276– 2284, https://doi.org/10.1175/1520-0469(1976)033<2276:VSOGWC>2.0.CO;2, 1976.

Fritts, D. C., and Luo, Z.: Gravity wave forcing in the middle atmosphere due to reduced ozone heating during a solar 320 eclipse. Journal of Geophysical Research, 98(D2), 3011– 3021. https://doi.org/10.1029/92JD02391, 1993.

Fritts, D. C., Vadas, S. L., Riggin, D. M., Abdu, M. A., Batista, I. S., Takahashi, H., Medeiros, A., Kamalabadi, F., Liu, H. L., Fejer, B. G., and Taylor, M. J.: Gravity wave and tidal influences on equatorial spread F based on observations during the Spread F Experiment (SpreadFEx), Ann. Geophys., 26, 3235–3252, https://doi.org/10.5194/angeo-26-3235-2008, 2008

Gossard, E., and Hooke, W.: Waves in the atmosphere: atmospheric infrasound and gravity waves- their generation and 325 propagation, Elsevier Scientific Publishing Co., 1975.

18

Hecht, J. H., Walterscheid, R. L., and Ross, M. N.: First measurements of the two-dimensional horizontal wave number spectrum from CCD images of the nightglow, Journal of Geophysical Research, 99(A6), 11449, https://doi.org/10.1029/94JA00584, 1994.

Hocking, W. K., Fuller, B., and Vandepeer, B.: Real-time determination of meteor-related parameters utilizing modern 330 digital technology, Journal of Atmospheric and Solar-Terrestrial Physics, 63(2–3), 155–169, https://doi.org/10.1016/S1364-6826(00)00138-3, 2001.

Krasovskij, V. I., and Šefov, N. N.: Airglow, J. Space Science Reviews, 4, 176-198, https://doi.org/10.1007/BF00173881, 1965.

Lighthill, J.: Waves in Fluids, Cambridge Univ. Press, New York, 1978.

335 Marlton, G. J., Williams, P. D., and Nicoll, K. A.: On the detection and attribution of gravity waves generated by the 20 March 2015 solar eclipse, https://doi.org/10.1098/rsta.2015.0222, 2016.

Marks, C. J., and Eckermann, S. D.: A Three-Dimensional Nonhydrostatic Ray-Tracing Model for Gravity Waves: Formulation and Preliminary Results for the Middle Atmosphere. J. Atmos. Sci., 52, 1959–1984, https://doi.org/10.1175/1520-0469(1995)052<1959:ATDNRT>2.0.CO;2, 1995.

340 Medeiros, A. F., Taylor M. J., Takahashi, H., Batista, P. P., and Gobbi, D.: An investigation of gravity wave activity in the low-latitude upper mesosphere: Propagation direction and wind filtering, Journal of Geophysical Research: Atmospheres, 108, https://doi.org/10.1029/2002JD002593, 2003.

Medeiros, A. F., Takahashi, H., Buriti, R. A., Fechine, J., Wrasse, C. M., and Gobbi, D.: MLT gravity wave climatology in the South America equatorial region observed by airglow imager, Annales Geophysicae, 25, 399–406, 345 https://doi.org/10.5194/angeo-25-399-2007, 2007.

Mertens, C. J., Mlynczak, M. G., López-Puertas, M., Wintersteiner, P. P., Picard, R. H., Winick, J. R., Gordley, L. L., and Russell III, J. M.: Retrieval of mesospheric and lower thermospheric kinetic temperature from measurements of CO_2 15 μm Earth Limb Emission under non-LTE conditions, Geophysical Research Letters, 28, 1391–1394, https://doi.org/10.1029/2000GL012189, 2001.

350 Nyassor P. K., Buriti, R. A., Paulino, I., Medeiros, A. F., Takahashi, H., Wrasse, C. M., and Gobbi, D.: Determination of gravity wave parameters in the airglow combining photometer and imager data. Annales Geophysicae, 36(3), 705–715, https://doi.org/10.5194/angeo-36-705-2018, 2018.

Paulino, A., Batista, P., Lima, L., Clemesha, B., Buriti, R., and Schuch, N.: The lunar tides in the mesosphere and lower thermosphere over Brazilian sector, Journal of Atmospheric and Solar-Terrestrial Physics, 133, 129–138, 355 https://doi.org/10.1016/j.jastp.2015.08.011, 2015.

Paulino, A. R., Batista, P. P., and Batista, I. S.: A global view of the atmospheric lunar semidiurnal tide, Journal of Geophysical Research: Atmospheres, 118, 13,128–13,139, https://doi.org/10.1002/2013JD019818, 2013.

Paulino, I., Medeiros, A., Buriti, R., Sobral, J., Takahashi, H., and Gobbi, D.: Optical observations of plasma bubble westward drifts over Brazilian tropical region, Journal of Atmospheric and Solar-Terrestrial Physics, 72, 521–527, 360 https://doi.org/10.1016/j.jastp.2010.01.015, 2010.

Paulino, I., Takahashi, H., Vadas, S., Wrasse, C., Sobral, J., Medeiros, A., Buriti, R., and Gobbi, D.: Forward ray-tracing for medium-scale gravity waves observed during the {COPEX} campaign, Journal of Atmospheric and Solar-Terrestrial Physics, 90-91, 117–123, https://doi.org/10.1016/j.jastp.2012.08.006, 2012.

Paulino, I., Moraes, J. F., Maranhão, G. L., Wrasse, C. M., Buriti, R. A., Medeiros, A. F., Paulino, A. R., Takahashi, H., 365 Makela, J. J., Meriwether, J. W., and Campos, J. A. V.: Intrinsic parameters of periodic waves observed in the OI6300 airglow layer over the Brazilian equatorial region, Annales Geophysicae, 36, 265–273, https://doi.org/10.5194/angeo-36-265-2018, 2018.

Picone, J. M., Hedin, A. E., Drob, D. P., and Aikin, A. C.: NRLMSISE-00 empirical model of the atmosphere: Statistical comparisons and scientific issues, J. Geophys. Res., 107, 1468, 0148-0227, https://doi.org/10.1029/2002JA009430, 2002.

370 Plougonven, R., Jewtoukoff, V., Cámara, A., Lott, F., and Hertzog, A.: On the Relation between Gravity Waves and Wind Speed in the Lower Stratosphere over the Southern Ocean, Journal of the Atmospheric Sciences, 74, 1075–1093, https://doi.org/10.1175/JAS-D-16-0096.1, 2017.

Pramitha, M., Venkat Ratnam, M., Taori, A., Krishna Murthy, B. V., Pallamraju, D., and Vijaya Bhaskar Rao, S.: Identification of gravity wave sources using reverse ray tracing over Indian region, Journal of Atmospheric Chem. Phys., 14, 375 19587-19623, https://doi.org/10.5194/acpd-14-19587-2014, 2014.

Press, W. H., Brian P. F., Saul A. T., and William T. V.: Numerical recipes: The Art of scientific computing, Cambridge University Press, 3, New York, 2007.

Sarkar, S., and Scotti, A.: Topographic Internal Gravity Waves to Turbulence, Annual Review of Fluid Mechanics, 49(1), 195–220. https://doi.org/10.1146/annurev-fluid-010816-060013, 2017.

380 Sivakandan, M., Paulino, I., Taori, A., and Niranjan, K.: Mesospheric gravity wave characteristics and identification of their sources around spring equinox over Indian low latitudes, 9(1), 93–102, https://doi.org/10.5194/amt-9-93-2016, 2016.

Sivjee G. G.: Airglow hydroxyl emissions, Planetary and Space Science, 40, 235-242, https://doi.org/10.1016/0032-0633(92)90061-R., 1992.

Taylor M. J., Pautet P. D., Medeiros A., Buriti R., Fechine J., Fritts D., Vadas S., Takahashi H., and Sao Sabbas F.: 385 Characteristics of mesospheric gravity waves near the magnetic equator, Brazil, during the SpreadFEx campaign. Annales Geophysicae, 27, 461–472, https://doi.org/10.5194/angeo-27-461-2009, 2009

Vadas, S. L., and Fritts, D. C.: Thermospheric responses to gravity waves: Influences of increasing viscosity and thermal diffusivity, Journal of Geophysical Research: Atmospheres, 110, https://doi.org/10.1029/2004JD005574, 2005.

Vadas, S. L.: Horizontal and vertical propagation and dissipation of gravity waves in the thermosphere from lower 390 atmospheric and thermospheric sources, Journal of Geophysical Research: Space Physics, 112, https://doi.org/10.1029/2006JA011845, 2007.

Vadas, S. L., and Liu, H.: Generation of large-scale gravity waves and neutral winds in the thermosphere from the dissipation of convectively generated gravity waves, *J. Geophys. Res.*, 114, https://doi.org/10.1029/2009JA014108, 2009

Vadas, S. L., and Fritts, D. C.: Reconstruction of the gravity wave field from convective plumes via ray tracing, Annales
395 Geophysicae, 27, 147–177, https://doi.org/10.5194/angeo-27-147-2009, 2009.

Vadas, S. L., Taylor, M. J., Pautet, P. D., Stamus, P. A., Fritts, D. C., Liu, H.L., São Sabbas, F. T., Rampinelli, V. T., Batista,
P., and Takahashi, H.: Convection: the likely source of the medium-scale gravity waves observed in the OH airglow layer
near Brasilia, Brazil, during the SpreadFEx campaign, Annales Geophysicae, 27, 231–259, https://doi.org/10.5194/angeo-27-
231-2009, 2009.

400 Vargas, F., Gobbi, D., Takahashi, H., and Lima, M.: Gravity wave amplitudes and momentum fluxes inferred from OH
airglow intensities and meteor radar winds during SpreadFEx, Ann. Geophys., 27(6), 2361–2369,
https://doi.org/10.5194/angeo-27-2361-2009, 2009

Wallace, L., and Chamberlain J. W.: Excitation of O2 atmospheric bands in the aurora, Planetary and Space Science, 2, 60-
70, https://doi.org/10.1016/0032-0633(59)90060-1, 1959.

405 Wrasse, C. M., Nakamura, T., Takahashi, H., Medeiros, A. F., Taylor, M. J., Gobbi, D., Denardini, C. M., Fechine, J., Buriti,
R. A., Salatun, A., Suratno, A., Achmad, E., and Admiranto, A. G.: Mesospheric gravity waves observed near equatorial and
low and middle latitude stations: wave characteristics and reverse ray tracing results, Annales Geophysicae, 24, 3229–3240,
https://doi.org/10.5194/angeo-24-3229-2006, 2006.

21